


Visual awareness sharpens and accelerates attentional sampling through enhancing inhibitory neural modulation in the attention network

Received: 8 December 2024

Fang Yang^{1,2}, Peijun Yuan^{1,2}, Li Shen^{1,2}, Ke Zhou³, Sheng He^{2,4} & Yi Jiang^{1,2} 

Accepted: 29 September 2025

Published online: 17 November 2025


 Check for updates

Attentional sampling, orchestrated by neural oscillations within the frontoparietal attention network, sequentially focuses on stimuli in a dynamic pattern, thereby enhancing the efficiency of attentional selection. However, the role of conscious awareness in this default attentional process remains largely unexplored. Here, we employed the Chromatic Flicker Fusion (CFF) method to render attentional cues invisible and investigated how cue awareness modulates attentional sampling. Using a high-temporal-resolution behavioral paradigm and electroencephalography (EEG) combined with the temporal response function (TRF) approach, we found that both visible and invisible cues induced rhythmic behavioral sampling and reset connectivity between the frontal and right occipito-parietal regions, indicating that attention samples rhythmically regardless of cue awareness. Crucially, visible cues not only elicited stronger behavioral inhibition and enhanced neural alpha activity, but also triggered faster attentional sampling (~8 Hz vs. ~4 Hz) and higher-frequency frontoparietal coupling (alpha vs. theta band). These findings demonstrate that the conscious representation of attentional cues influences inhibitory neural responses within the frontoparietal attention network and modulates the attentional sampling process.

Our brain is constantly bombarded with sensory inputs, and selective attention acts as a filtering mechanism to enhance relevant information while suppressing irrelevant details based on their salience or task-related values. This process enhances sensory processing and leads to improved behavioral outcomes, as evidenced by higher hit rates and faster reaction times¹.

Traditionally, models of attention have remained agnostic about whether sustained selective attention operates continuously over time or follows a more dynamic, fluctuating pattern. Recent evidence

supports the latter, revealing the rhythmic property of attention^{2,3}. Behavioral studies have shown that when new stimuli direct attention to a specific location, object, or feature, individuals' performance fluctuates at low frequencies, primarily within the theta (3–7 Hz) and alpha (8–12 Hz) bands^{4–7}. These fluctuations suggest that attention periodically explores the visual scene at theta and alpha frequencies after being reset to that position, object, or feature^{2,3,8}. The rhythmic property of attention may prevent prolonged fixation in one place and facilitate efficient exploration of the environment^{6,9}. However, this

¹State Key Laboratory of Cognitive Science and Mental Health, Institute of Psychology, Chinese Academy of Sciences, Beijing, PR China. ²Department of Psychology and College of Life Science, University of Chinese Academy of Sciences, Beijing, PR China. ³Beijing Key Laboratory of Applied Experimental Psychology, National Demonstration Center for Experimental Psychology Education (Beijing Normal University), Faculty of Psychology, Beijing Normal University, Beijing, PR China. ⁴State Key Laboratory of Cognitive Science and Mental Health, Institute of Biophysics, Chinese Academy of Sciences, Beijing, PR China.  e-mail: yijiang@psych.ac.cn

interpretation has been questioned. Recent studies highlight that earlier research did not adequately differentiate periodic from aperiodic temporal dynamics, raising the possibility that observed oscillations partly reflect aperiodic temporal structures¹⁰. Whether attention truly samples the environment in a periodic fashion and whether this process reliably manifests at specific frequencies remains a critical, open question.

Despite ongoing debate over the existence of behavioral rhythms, accumulating evidence suggests that attentional sampling of the environment is governed by neural mechanisms closely tied to brain oscillations. Recent electrophysiological studies have demonstrated that fluctuations in behavioral performance align with oscillatory activities in the alpha and theta frequency bands within the frontoparietal network. In particular, occipito-parietal alpha oscillations have long been associated with attentional selection, with higher power leading to improved distractor suppression¹¹. Moreover, the phase of alpha oscillations at stimulus onset has been linked to fluctuations in perception and behavioral performance^{12,13}. Alpha rhythm in the prefrontal area has also been proposed as a key regulator of attentional sampling⁶.

Another crucial mechanism for attentional sampling lies in the theta rhythm. For instance, the synchronization of theta phase within the frontoparietal network, potentially involving intricate interactions with the mediodorsal pulvinar, has been proposed as a potential mechanism of attentional sampling^{14,15}. Additionally, the modulation of alpha power by theta phase has been observed in both behavioral performance¹⁶ and neural impulse responses¹⁷. This evidence suggests that attentional sampling is correlated with multiple rhythmic generators and complex network interactions.

Despite the increasing research on the rhythmic mechanisms of attention, our understanding of its relationship with visual awareness remains limited. On the one hand, rhythmic sampling has been considered an inherent state or default mode of attention^{6,8,15,18}, leading to the possibility that it may be unaffected by visual awareness. Indeed, growing evidence suggests that many aspects of selective attention, particularly bottom-up selection driven by salience or sudden stimulus onset, can be dissociated from visual awareness of the stimulus^{19,20}. On the other hand, the emergence of visual awareness often involves a deeper and more prolonged propagation of activation through long-distance connections between brain regions compared to unconscious states²¹. Therefore, it is reasonable to posit that visual awareness of a stimulus is vital for the establishment of connectivity within the frontoparietal attention network, thereby modulating the operation of attentional sampling. However, there is currently no empirical behavioral or neural evidence to disentangle these conflicting views.

To fill this gap, we investigated whether objective visual awareness of attentional cues influences the temporal dynamics of attention. Specifically, we conducted two Posner cueing tasks, where subjects were instructed to covertly attend to two placeholders simultaneously and discriminate or detect an upcoming target. Visible or invisible cues were used to direct their attention to specific stimuli. We adopted a two-alternative forced choice task to ensure that invisible cues were presented below the objective threshold, defined as the inability to detect the location of cues above chance level. Unlike subjective visibility rating or meta-cognitive confidence measures, this approach tests whether stimuli meet the criteria of fully unconscious processing²². During the task, we rendered the cue invisible using the Chromatic Flicker Fusion (CFF) method^{23–27}, in which two oppositely colored stimuli (e.g., red and green) were alternately presented at a temporal frequency above the fusion threshold (~30 Hz). The CFF cue perceptually fused into a color (e.g., yellow) that is indistinguishable from the background, rendering it invisible to conscious awareness. This method offers a unique advantage by enabling the presentation of both invisible and visible stimuli to both eyes for the same duration and intensity without any masking.

We explored the behavioral attentional fluctuation induced by different cues using a high-temporal-resolution behavioral paradigm (Experiment 1, with target presented at 28 temporal intervals following the cues). The time series of observed attentional effects were decomposed into a slowly evolving trend component and a rapidly fluctuating component (Fig. 1a). Using both autoregressive (AR) surrogate¹⁰ and time randomization method⁷, the significance of the rhythmic component was then assessed after accounting for aperiodic influences (Fig. 2). Then, we delved into the underlying neural mechanisms using EEG techniques combined with a temporal response function (TRF) method (Experiment 2). As shown in Fig. 1b, this approach allowed us to extract object-specific (cued and uncued) neural impulse responses from EEG signals²⁸. Here, we show that cue awareness not only strengthens inhibitory responses in behavior and neural activity but also accelerates attentional sampling and shifts frontoparietal connectivity from theta to alpha rhythms.

Results

None of the subjects reported perceiving the cues rendered invisible using the CFF method (i.e., invisible cues). However, they were able to report the presence of visible cues. In the two-alternative forced-choice task assessing objective cue awareness, their performance in localizing the invisible cues did not significantly differ from chance level (See Supplementary Table 1; all p s > 0.100), indicating that they were unaware of the presence of the invisible cues. These results suggest that the CFF method effectively manipulated the cue awareness.

Visible cues evoked more pronounced inhibition effect than invisible cues

The subjects' reaction times (RTs) to the targets were measured. We decomposed the time course of the difference in normalized RTs between the cued and uncued targets (i.e., cueing effect, CE) into slowly evolving trends and rhythmic sampling (Fig. 1a). In line with previous studies^{16,29}, the smoothed trend exhibited classical early facilitation and later inhibition for the visible condition (Fig. 3b). Subjects responded faster to targets presented on the same side as the cues than those on the opposite side during short SOAs (167–400 ms), but this pattern reversed during longer SOAs (733–900 ms). In contrast, the smoothed profiles in the invisible condition only revealed early facilitation (233–267 ms).

To directly compare the facilitation and inhibition effects across conditions, we conducted a two-way ANOVA (cue visibility × SOA window) on the averaged CE (Fig. 3b). The analysis revealed a significant interaction effect ($F(1,19) = 4.83$, $p = 0.041$, $\eta_p^2 = 0.20$). Simple main effects analysis indicated that the facilitation effects did not significantly differ between the visible and invisible conditions ($t(19) = 1.27$, $p_{\text{uncorr}} = 0.221$, Cohen's $d = 0.28$, $CI = [-0.017, 0.067]$, $BF_{10} = 0.47$). However, the inhibition effect in the visible condition was significantly stronger than in the invisible condition ($t(19) = -2.26$, $p_{\text{uncorr}} = 0.036$, Cohen's $d = -0.51$, $CI = [-0.131, -0.005]$, $BF_{10} = 1.81$). Consistent with prior research^{30,31}, our results indicated that both visible and invisible cues automatically captured attention, leading to early perceptual enhancement at cued locations (See Supplementary Fig. 1 for further evidence of early facilitation induced by invisible cues). Furthermore, the significant difference in the inhibition effect suggests that visible cues induced stronger inhibition at the previously attended location, a phenomenon known as inhibition of return (IOR)³².

Visible cues induced faster attentional sampling than invisible cues

We then examined attentional sampling by translating the detrended CE time courses into the frequency domain using the fast Fourier transform (FFT)^{16,29}. As depicted in Fig. 3c, the group-averaged power spectrum for different cues exhibited distinct peaks at different frequencies. Specifically, the invisible condition induced a significant peak at 3.75 Hz ($p_{\text{max}} < 0.050$; for both AR-based and randomization-

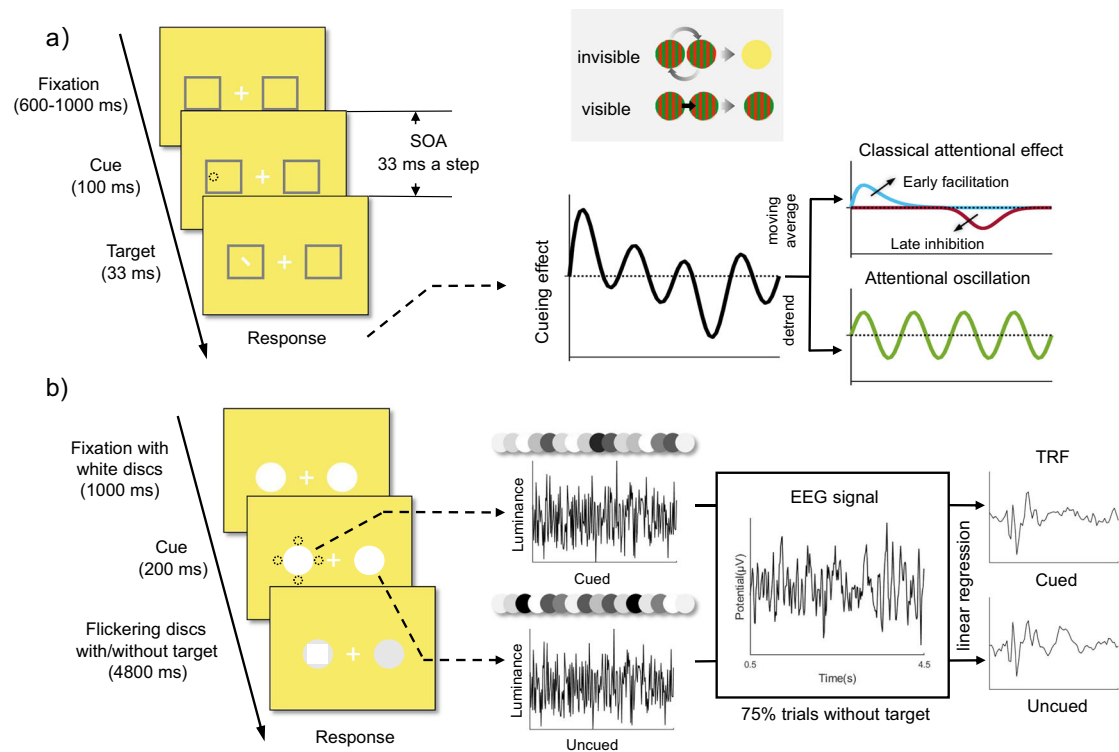


Fig. 1 | Illustration of stimuli and procedure for all experiments. **a** In Experiment 1, participants fixated on a central cross and covertly attended to two placeholders. A cue then appeared at the periphery of one of the two placeholders, with a 50% congruency to the target location, directing attention to the left or right. In the invisible condition, the cues consisted of two anti-phased red-and-green sinusoidal grating discs alternating at 30 Hz, which fused into a yellow disc indistinguishable from the background. In the visible condition, one of the gratings was randomly selected and presented continuously. To densely sample behavioral performance, the target line appeared at one of 28 stimulus onset asynchronies (SOAs), ranging from 0.1 to 1 s after cue onset, in 33 ms steps. Participants responded as quickly and accurately as possible by pressing the corresponding keys to indicate the tilt direction of the target. Cueing effects were analyzed by decomposing them into

classical early facilitation, late inhibition, and attentional oscillation. **b** In Experiment 2, at cue onset, the luminance of two placeholder discs was independently modulated using customized sequences that updated with each frame refresh. On 25% of the trials, a target square was presented for 0.5 s at a random time during the flickering. Its luminance contrast relative to the placeholder disc was adjusted across trials using a 3-down-1-up staircase procedure. After the flickering ended, participants pressed the corresponding keys to report whether they detected the target. EEG signals and luminance sequences without the target were used to estimate the object-specific neural impulse response using the Temporal Response Function (TRF) technique. *Note:* Stimulus colors and sizes in the figure are illustrative and do not reflect actual stimuli used in the experiments.

based methods), while the visible condition showed a significant peak at 7.50 Hz ($p_{\max} < 0.050$; for both AR-based and randomization-based methods). Similar patterns were found in the time course of normalized RT on the uncued targets (See Supplementary Fig. 2; visible condition peaked at 7.97 Hz; invisible condition peaked at 4.69 Hz). These results indicate that attention exhibits behaviorally measurable oscillations predominantly in the theta range, even after accounting for aperiodic components. The effect is especially pronounced at uncued locations requiring attentional reorienting, consistent with previous findings^{33,34}.

In light of the distinct peak frequencies observed in the attentional oscillatory spectra across levels of cue awareness, we extracted the individual peak frequencies within the 3–10 Hz range to directly compare attentional sampling rates between conditions (Fig. 3e). The individual peak frequencies for the visible condition were significantly higher than those for the invisible condition (7.22 Hz vs. 5.93 Hz, $t(19) = 2.33$, $p = 0.031$, Cohen's $d = 0.52$, $CI = [0.133, 2.450]$, $BF_{10} = 2.04$). These results suggest that attentional sampling induced by visible cues was faster than that induced by invisible cues.

To further compare the phase of attentional sampling under different conditions, we conducted phase analysis on the cued and uncued RT time courses within the two peak oscillation bands (3.5–4.5 Hz & 7–8 Hz). As shown in Fig. 3d, for the 3.5–4.5 Hz band, the individual phase lags between the cued and uncued RT time courses of the invisible condition were clustered around 214.9° ($p_{\text{uncorr}} = 0.020$,

$r_{\text{ay}} = 0.44$), and this distribution was significantly different from the visible condition ($p_{\text{uncorr}} = 0.006$, $U^2 = 0.26$). However, for the 7–8 Hz band, the cued-uncued phase lags were more clustered under the visible condition (mean = 124.7°; $p_{\text{uncorr}} = 0.004$, $r_{\text{ay}} = 0.51$) than the invisible condition ($p_{\text{uncorr}} = 0.003$, $U^2 = 0.30$). V-test results further revealed that phase lags in the 3.5–4.5 Hz range under the invisible condition ($v = 7.19$, $p_{\text{uncorr}} = 0.011$), as well as those in the 7–8 Hz range under the visible condition ($v = 5.80$, $p_{\text{uncorr}} = 0.033$), were significantly clustered around 180°, indicating an alternating attentional sampling between cued and uncued locations. These findings also suggest that the phase reset of attentional sampling occurred at distinct frequencies for the visible and invisible conditions, providing additional evidence that visible and invisible cues modulate attentional sampling dynamics differently. To minimize late-stage RT noise, phase analysis was restricted to data before 800 ms. Extending the analysis beyond 850 ms revealed no significant phase clustering, due to increased preparatory and additional cognitive processes that obscured phase resetting effects.

In previous studies, the analysis of attentional sampling often excluded the trends of facilitation and inhibition effects, leaving the interplay between these processes unexplored^{7,16}. We conducted a correlation analysis between the strength of inhibitory cueing effects and individual attentional sampling frequencies. There was a correlation trend, particularly in visible conditions (Fig. 3f, $r(18) = -0.40$, $p_{\text{uncorr}} = 0.085$), suggesting that the stronger inhibitory cueing effects,

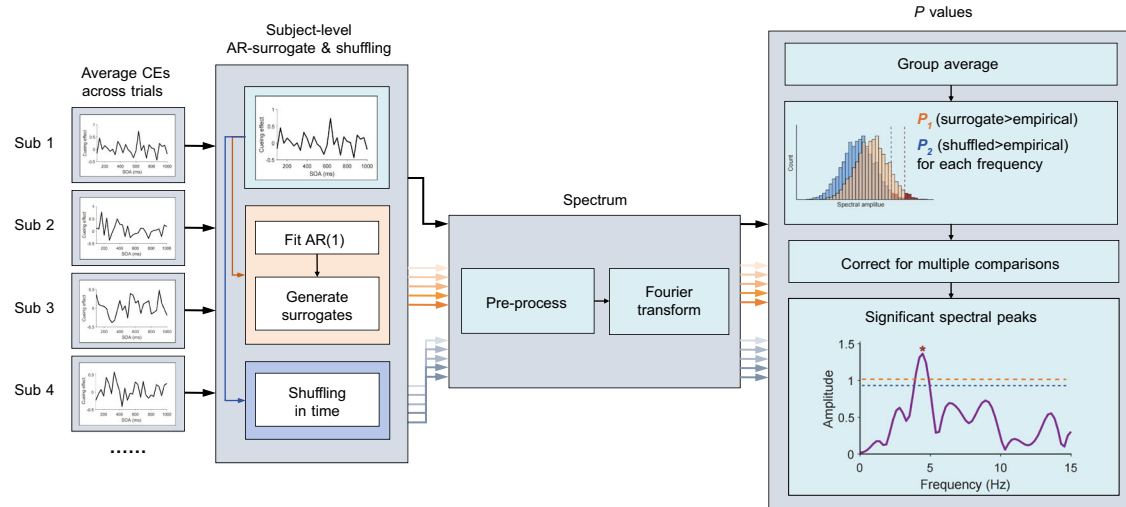


Fig. 2 | Schematic of the behavioral oscillation analysis pipeline. To identify true periodic components in cue-related behavioral dynamics, we implemented two parallel statistical approaches: (1) For each participant, cueing effects (CEs) time series were constructed by averaging across trials. (2) An autoregressive (AR) model was fitted to the time series for each subject to model aperiodic trends. Based on these AR models, we generated 1000 surrogate datasets to create a null distribution of group-level spectra reflecting aperiodic structure only. (3) In

parallel, we applied a randomization-based approach by shuffling each participant's time series 1000 times, yielding a second null distribution that disrupted all consistent temporal structure. (4) Empirical spectra were computed and compared to both null distributions. Surpassing the AR-based threshold indicated true periodicity beyond aperiodic trends, while exceeding the randomization-based threshold reflected existing of time-locked patterns.

the faster attention sampled across space locations. This result implies that the traditional IOR and rhythmic sampling could represent a shared dynamic mechanism inherent in the attention system.

Visible cues elicited stronger inhibitory alpha power than invisible cues

The behavioral results from the EEG experiment, together with those from the supplementary experiment, indicate that cue awareness also modulates the attentional effect on target perceptual thresholds (Supplementary Fig. 3). To further investigate the underlying neural mechanisms, we applied the TRF method to extract the neural impulse responses as a function of time lag (−100 to 1000 ms) for cued and uncued disc sequences from EEG recordings (see Methods). The TRF became flat and noisy when the relationship between the stimulus sequence and EEG recording was shuffled (Fig. 4a, black vs. yellow line), suggesting that the estimated TRF represented a stimulus-specific neural response.

Following spectral analysis of the TRF, we computed the group-averaged power across all experimental conditions and electrode sites. This analysis revealed increased power spectral density in both the alpha (8–12 Hz) and theta (4–8 Hz) frequency bands during the 117–383 ms time lags (Fig. 4b). Based on these temporal dynamics, we defined this interval as the time window of interest (TOI) for subsequent analyses. We then conducted condition-specific statistical comparisons to assess differences in alpha and theta oscillatory power between cued and uncued conditions. Both visible and invisible cues modulated alpha power rather than theta power (see Supplementary Fig. 4 for theta-band results). Figure 4c displays the topography of the significant alpha power modulation effects. Under the invisible condition, the alpha power of the cued TRF was weaker than that of the uncued TRF over the right occipito-parietal electrodes ($p_{\text{max-cluster}} = 0.033$; PO6, PO8, P6). In contrast, under the visible condition, the modulation of alpha power was reversed (cued > uncued) at two electrode clusters located in the frontal ($p_{\text{max-cluster}} = 0.005$; F3, F1, FC5, FC3, FC1, C1) and right occipito-parietal ($p_{\text{max-cluster}} = 0.003$; O2, PO4, PO6, PO8, P4, P6, P8) regions.

To further assess awareness-related alpha power modulation, we compared the cueing effect (i.e., CE_{alpha} , calculated as cued minus uncued conditions) between visible and invisible conditions, both

within the TOI and across the full 0–1000 ms post-cue time interval. These analyses identified two significant spatial clusters (Fig. 4c)—one in the mid-frontal ($p_{\text{max-cluster}} < 0.050$ for both methods; AF4, F4, F2, F3, FC3, F1) and another in the right occipito-parietal region ($p_{\text{max-cluster}} < 0.050$ for both methods; Oz, O2, PO4, PO6, PO8, P6, P8). These clusters, which were consistently observed across both the full-time windows and the predefined TOI, were subsequently defined as channels of interest (COI). Moreover, the significant temporal cluster identified in the full-time window analysis (167–267 ms) fell within the TOI. These findings demonstrate distinct neural dynamics for visible versus invisible cues across frontal and occipito-parietal networks.

We analyzed the CE_{alpha} time courses for the visible and invisible conditions within the two COI clusters. As shown in Fig. 4d, in the mid-frontal region, only visible cues induced a significant increase in CE_{alpha} (167–250 ms), while invisible cues showed no significant effect. In the right occipito-parietal region, both visible and invisible cues induced significant CE_{alpha} , but in opposite directions: visible cues induced increased CE_{alpha} (167–267 ms), whereas invisible cues induced decreased CE_{alpha} (217–250 & 383–417 ms). Notably, in both regions, CE_{alpha} was significantly stronger in the visible than in the invisible condition during the 167–267 ms time window, consistent with our cluster-based analysis. These findings suggest that invisible cues only elicit a facilitation effect at the right-lateralized occipito-parietal region, as indicated by lower alpha power for cued stimuli relative to uncued ones. In contrast, the CE_{alpha} induced by visible cues resembles that observed in previous studies¹⁷, showing increased alpha power over cued stimuli in the frontoparietal region when the cues were irrelevant to the task.

To test whether the cue-induced CE_{alpha} reflects the inhibition function of attention, we calculated the correlation coefficients between behavioral performance and CE_{alpha} across individual subjects. The behavioral index (i.e., $CE_{\text{threshold}}$) reflected the difference in the contrast threshold required for accurate detection of targets presented on the cued versus uncued discs. Meanwhile, the CE_{alpha} reflects the difference in alpha power between the cued and uncued conditions. We observed trends of negative correlation between these two indices across both clusters and for both cues, and this negative

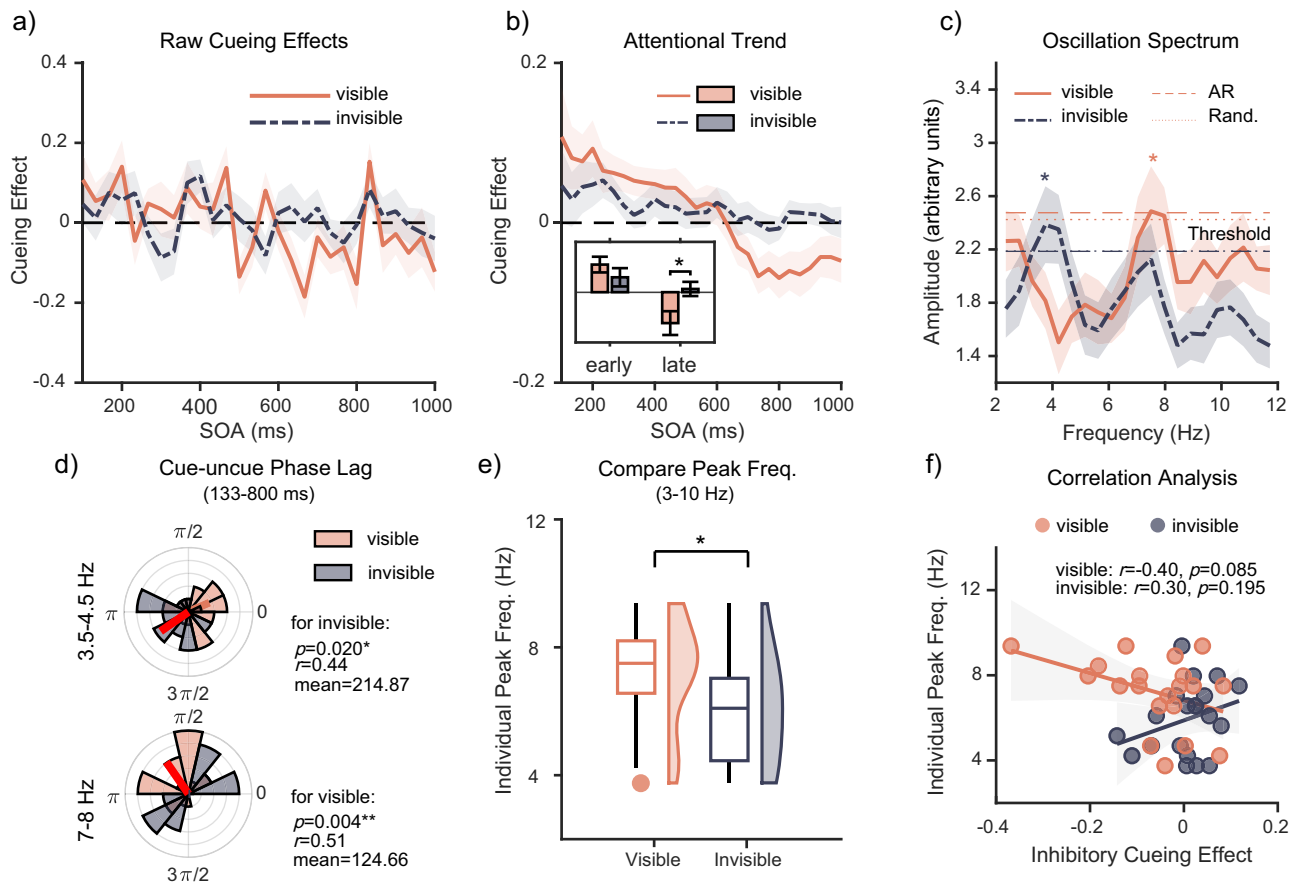


Fig. 3 | Results of Experiment 1. a Mean raw cueing effects (CEs) across stimulus onset asynchronies (SOAs) for the visible and invisible conditions. **b** Mean CEs after applying a sliding-window average across SOAs. Bar plots show mean early (100–400 ms SOAs) and late (600–1000 ms SOAs) CEs for both conditions. A significant difference was found in the late CEs between conditions ($p = 0.036$, two-tailed paired t -test, uncorrected). **c** Mean power spectra of detrended CEs computed via fast Fourier transform (FFT). Power peaks emerged at -8 Hz for the visible condition and -4 Hz for the invisible condition. Horizontal dashed lines indicate significance thresholds derived from AR-based (AR) and randomization-based (rand.) test ($p = 0.05$, one-tailed; corrected using the max-value method). Spectral peaks exceeding both thresholds are marked with asterisks. **d** Distributions of phase lag between cued and uncued response-time-based oscillations in the 3.5–4.5 Hz and 7–8 Hz frequency bands (within the 133–800 ms post-cue interval). Red lines indicate the mean phase lag where significant clustering was found ($p < 0.05$, Rayleigh test; uncorrected). **e** Individual peak frequencies (freq.) selected

within 3–10 Hz range for each condition. Boxes indicate the interquartile range, whiskers extend to data range excluding outliers, and the center lines denote the median. Shaded violins show full distribution of the data. Peak frequencies were significantly higher in the visible condition compared to the invisible condition ($p = 0.031$; two-tailed paired t -test). **f** Scatter plot showing the relationship between individual peak frequency and the magnitude of the inhibitory cueing effect. Each dot represents one participant for each condition. Linear regression lines were shown with shaded regions indicating 95% confidence intervals. A negative correlation trend was observed for the visible condition (Pearson correlation test; two-tailed, uncorrected). All statistical analyses were based on data from $N = 20$ participants (10 females, mean age 24.5 ± 2.8 ; within-subject design). All error bars and shaded areas indicate \pm SEM unless otherwise specified. Results for the visible and invisible conditions are consistently indicated using orange and gray, respectively. * $p < 0.05$; ** $p < 0.01$. Source data are provided as a Source Data file.

correlation was particularly pronounced for the visible condition in the right occipito-parietal region (see Supplementary Fig. 5; $r(20) = -0.68$, $p_{\text{uncorr}} < 0.001$). These results suggest that the stronger the alpha power for the cued TRF relative to the uncued TRF, the poorer the detection performance on the cued disc relative to the uncued disc, supporting the assumption of an inhibitory function of alpha power.

Cue awareness modulated connectivity between frontal and right occipito-parietal regions

Previous electrophysiological studies have demonstrated that phase synchronization between the frontal and parietal regions could serve as a crucial mechanism for attentional sampling. When the cue appeared, the consistency of phase difference within the theta band between the frontal and parietal areas was significantly enhanced¹⁴. Considering that the alpha power modulation in our study involved two distinct regions of frontal and right-lateralized parietal attention networks, we proceeded to conduct a phase-based connectivity analysis between these two regions.

Figure 4e demonstrates the differences in phase-locking value (PLV) of the frontal and right occipito-parietal clusters between the cued and uncued conditions. We observed a stronger PLV in the cued than the uncued condition. Notably, the largest cluster showing a pronounced difference in PLV ($p_{\text{max-pixel}} < 0.025$) was concentrated within the time lag of 450–900 ms in the theta band (6–7 Hz) for the invisible condition. However, the largest cluster was concentrated within the time lag of 100–467 ms in the alpha band (9–14 Hz) for the visible condition. These results indicate that the visual awareness of cues influenced the neural connectivity between the frontal and parietal attention regions.

The Granger causality analysis focused on cued condition, which measures the influence that one brain region has on another, provides additional insights (Fig. 4f). The frontal region's influence on the right occipito-parietal region significantly peaked at 6 and 12 Hz ($p_{\text{max}} < 0.05$) for the invisible and visible conditions, respectively. These findings suggest that the connectivity between the frontal and occipito-parietal regions was primarily influenced by top-down

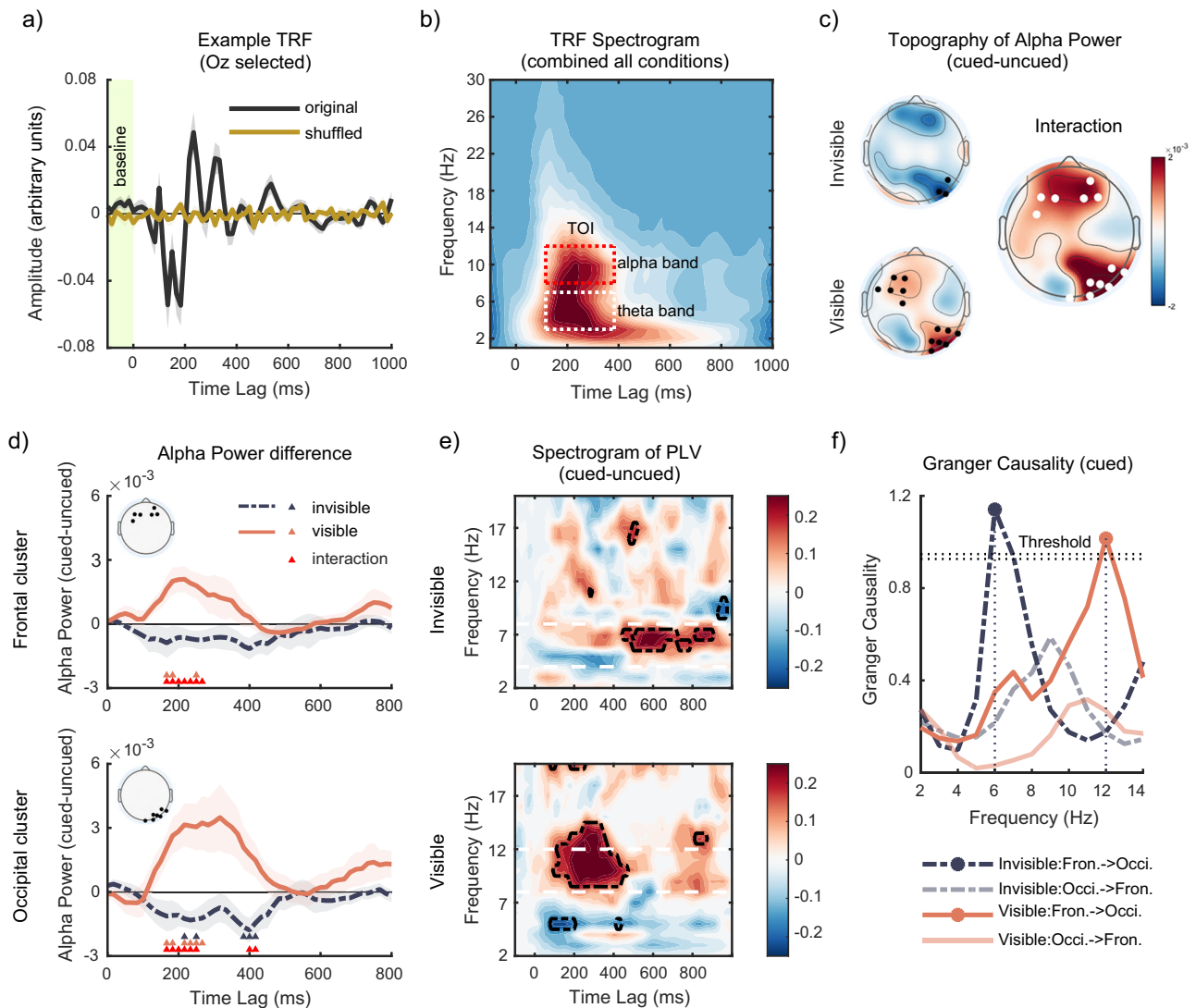


Fig. 4 | Results of Experiment 2. **a** Temporal response functions (TRFs) at electrode Oz, estimated using stimuli intensity profiles, are shown as mean \pm SEM. The TRF for actual stimuli (black line) resembles an ERP waveform, whereas the TRF for time-shuffled stimuli (yellow line) shows no discernible response. **b** Time-frequency representation (spectrogram) of TRFs pooled across all conditions and electrodes. Increased power is observed in the alpha (8–12 Hz; highlighted by red dash line) and theta (3–7 Hz; highlighted by white dash line) bands, particularly within 117–380 ms time lags (time of interests, TOI). **c** Topographic maps show alpha-band power differences between cued and uncued TRFs within the TOI for the invisible, visible and interaction effects. In the invisible condition, cued TRFs show reduced alpha power, whereas in the visible condition, alpha power is enhanced. Black dots mark electrodes with significant differences ($p < 0.05$, cluster-based permutation test, corrected using the Monte Carlo method). The larger map on the right depicts the interaction between visible and invisible conditions, with white dots indicating significant electrodes. **d** Time course of mean alpha power differences (cued vs.

uncued) induced by visible (orange line) and invisible (gray line) cues in frontal and occipito-parietal regions, shown as mean \pm SEM. Orange, gray, and red triangles denote time points with significant effects for the visible, invisible, and interaction contrasts, respectively ($p < 0.05$; two-tailed t -tests, FDR-corrected). **e** Spectrograms of phase-locking value (PLV) differences between cued and uncued TRFs for the invisible and visible conditions. Significant time-frequency clusters are outlined with dashed black lines ($p < 0.025$, permutation test, two-tailed, corrected using maximum pixel-based method). **f** Granger causality between frontal (fron.) and occipito-parietal (occi.) ROIs for cued TRFs under visible (orange) and invisible (gray) conditions. Darker lines represent frontal to occipito-parietal direction; lighter lines indicate the reverse. Horizontal dashed lines denote the significance threshold ($p = 0.05$, permutation test, two-tailed, corrected using max-value method). All statistical analyses were based on data from $N = 22$ participants (10 females, mean age 24.2 ± 3.1 ; within-subject design). Source data are provided as a Source Data file.

processes and operated at distinct frequencies depending on the visual awareness of cues.

Discussion

The present study aimed to elucidate the relationship between objective visual awareness of attentional cues and attentional sampling. Our findings indicate that both visible and invisible cues induced rhythmic sampling in the behavioral task, suggesting that rhythmic attentional sampling operates independently of consciousness. Notably, different cues induced different sampling patterns: visible cues

elicited stronger IOR and facilitated more rapid sampling (~ 8 Hz vs. ~ 4 Hz). Furthermore, visible cues enhanced inhibitory alpha oscillations in both the frontal and occipito-parietal regions, quickly establishing top-down alpha band connectivity (~ 12 Hz; 100–467 ms) between these areas. In contrast, invisible cues affected only alpha power in the occipito-parietal region, while enhancing theta band (~ 6 Hz) top-down connectivity between the frontal and occipito-parietal regions at a later time lag (450–900 ms). These findings suggest that the emergence of visual awareness for attentional cues influences the neural dynamics within the frontoparietal attention

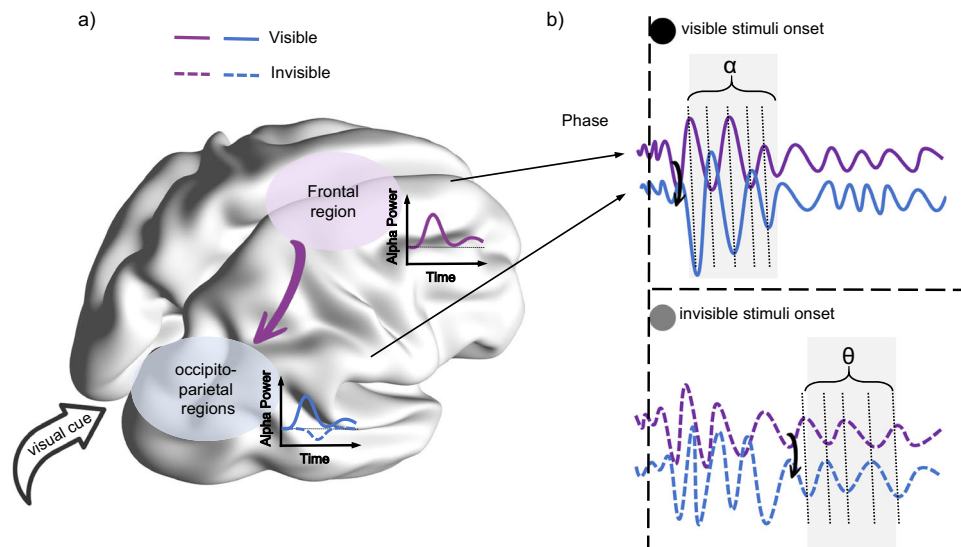


Fig. 5 | Illustration of how cue awareness modulates the temporal dynamics of attention. **a** When a cue is consciously perceived, its bottom-up attraction of attention could be successfully inhibited by the frontoparietal attention network, leading to stronger alpha oscillatory activity in both the frontal and occipito-parietal attention networks. **b** During this inhibition process, cue awareness also

influences the dynamic connectivity between the frontal and occipito-parietal attention networks. Specifically, the connection forms earlier and is primarily driven by alpha-band phase coherence due to top-down inhibition of visible cues. In contrast, without cue awareness, this connection is dominated by default top-down theta-band oscillations after the phase reset induced by cue onset.

network, modulating the attentional sampling process (as summarized in Fig. 5).

When attention is focused on a specific stimulus, perceptual resources are selectively exploited to analyze the attended stimulus, leaving other stimuli largely ignored. Attentional sampling plays a crucial role in creating windows of opportunity for disengaging from the current stimulus and shifting to a new one⁹. Growing evidence suggests that attention samples the visual scene at a theta rhythm^{4,5,7,35}, which is considered a fundamental property of attention.

However, whether such rhythmic properties are observable at the behavioral level—and whether they are genuinely oscillatory rather than driven by aperiodic temporal structures—remains a subject of ongoing debate¹⁰. In the present study, after controlling for aperiodic influences, we found that both visible and invisible attentional cues induced theta-band attentional fluctuation. These findings suggest that attention sampling is behaviorally measurable and operates independently of cue awareness, supporting the notion that theta band rhythmic sampling is an intrinsic property of the attentional system.

Even though the neural mechanism of attentional sampling is still under debate, some evidence suggests that large-scale inter-areal rhythmic coordination between the frontal and parietal regions plays an essential role³⁶. The theta phase-based connectivity from the frontal to parietal regions can mediate the conflict between the perceptual and oculomotor systems, supporting the alternation of attention exploitation and exploration^{14,15}. Additionally, theta phase has been associated with a reweighting of functional connections between cortical and subcortical hubs of the attention network³⁷. In line with these findings, we found that the theta band (6–7 Hz) phase-based connectivity from the frontal to occipito-parietal regions was enhanced by invisible cues. The frequency of this top-down connection is similar to the frequency of behavioral fluctuation. These findings, together with previous evidence, suggest that theta rhythmic frontoparietal connectivity plays a crucial role in attentional sampling even without cue awareness.

Although attentional sampling could operate regardless of whether the cues were consciously perceivable or not, the rates of attentional sampling were significantly different between the visible and invisible conditions. In the behavioral experiment, we found that

attentional sampling induced by visible cues was significantly faster than that induced by invisible cues (–8 Hz vs. –4 Hz). Furthermore, in the EEG experiment, we found that frontoparietal connectivity was established earlier (100–467 ms vs. 450–900 ms) and dominated by higher top-down frequencies (12 Hz vs. 6 Hz). These results suggest that visual awareness of stimuli can regulate the dynamics of attentional sampling.

While previous studies have primarily emphasized the role of the theta rhythm in attentional sampling, an increasing number of studies have found attentional sampling at higher frequencies. For example, when the task becomes simpler, the sampling between two locations becomes quicker^{34,38}. Additionally, when multiple spaces need to be sampled, attention also accelerates its sampling across space³⁹. A recent EEG study further demonstrated that the phase of pre-stimulus low-frequency oscillations predicts visual search performance, with the optimal sampling frequency shifting in accordance with task complexity⁴⁰. These findings highlight the adaptive nature of the neural mechanisms underlying attentional sampling, suggesting that the temporal dynamics of attention flexibly adjust to meet varying task demands. Before discussing how cue awareness modulates such flexibility, it is crucial to first examine the finding that cue awareness enhances the inhibitory function of attention.

There is substantial evidence suggesting that the abrupt onset of a new stimulus can capture attention in a bottom-up manner, leading to facilitation of performance⁴¹. However, if the new stimulus is known to be irrelevant to the task, this attentional capture is quickly suppressed, which can lead to worse performance at the already attended locations (known as IOR)³². Such facilitation and inhibition effects have long been envisioned as two inseparable sides of the same coin⁴². However, in our study, both visible and invisible cues induced facilitation effects, whereas only visible cues exhibited a suppression effect. The dissociation of facilitation and inhibition effects at different levels of cue awareness suggests that they may rely on independent mechanisms, consistent with recent findings^{43,44}.

One possibility is that the early facilitation observed at short SOAs reflects activation of the locus coeruleus–norepinephrine alerting system, triggered by the abrupt cue onset^{41,45}. Supporting this view, recent behavioral evidence suggests that briefly presented visual or auditory stimuli can enhance processing of targets appearing

within a continuously presented placeholder—a phenomenon termed rejuvenation⁴⁶. However, unlike these alerting paradigms, our task presented two simultaneous placeholders, with the cue appearing at only one location. If facilitation were driven solely by a non-specific alerting processing, target enhancement would be expected at both locations. Instead, we observed a robust spatial advantage for targets at the cued location, pointing to a mechanism beyond non-specific alerting and consistent with spatially selective attentional orienting. Crucially, the anti-phasic oscillatory pattern of reaction times between cued and uncued locations further supports a dynamic alternation between orienting and reorienting processes^{7,33}.

In human EEG and MEG studies, there exists a long-established correlation between attentional orienting and parietal alpha oscillations (8–12 Hz). Increased alpha synchrony is linked to attentional inhibition, while decreased alpha is associated with perceptual facilitation^{47–52}. Recent studies have also highlighted the close relationship between alpha oscillation in the TRF and the facilitation and inhibition of attention^{17,53}. They observed that when cues instructed subjects to maintain attention on a specific stimulus, the alpha-band power in its TRF decreased. Moreover, if the cue provided less task-relevant information, the alpha oscillation of the cued stimulus initially decreased and then increased. The authors suggested that this pattern of alpha oscillation, decreasing followed by increasing, reflected the dynamic shift of attention between cued and uncued stimuli.

In our study, invisible cues induced a decrease in alpha oscillations in the cued TRF, localized to the right-lateralized occipito-parietal region. Combining evidence from previous TRF studies, the reduced alpha oscillation might reflect facilitation of attention towards the cued stimuli. The right lateralization of this modulation is also consistent with previous findings demonstrating the dominance of the right hemisphere in bottom-up attentional orienting^{54–56}. Previous studies have shown that the activation from invisible CFF stimuli was limited to areas from V1 to V4^{25,57}. Therefore, our study also indicates that saliency encoding in the visual cortex^{58–61} is sufficient to activate the right-lateralized bottom-up attention system.

However, when the cue was consciously perceived, it elicited stronger alpha inhibition on the cued stimuli in the right occipito-parietal and frontal regions, leading to poorer performance in detecting the cued target. This observation, similar to prior studies, reflects the inhibition of irrelevant cues by the frontoparietal attention system. Moreover, we observed that the frontal region rapidly established a top-down alpha connection to the lower-order region. The frontal region is widely recognized as the primary area involved in top-down attention regulation^{62,63}. Neurons within the prefrontal region can generate attentional templates in the form of working memory representations, which are used to suppress irrelevant distractors based on the current template⁶⁴. This top-down control may be achieved through synchronization of rhythms in the upper alpha/lower beta band^{65,66}. Furthermore, the Global Neuronal Workspace theory suggests that top-down signals related to working memory originating from the frontal region depend on the availability of consciousness⁶⁷. Our findings support this speculation, indicating that top-down control over bottom-up attention capture is consciousness-dependent.

Fiebelkorn and Kastner⁹ proposed that IOR and attentional sampling might share the same neural basis, with some evidence indicating they have overlapping sources in the parietal cortex^{37,68}. Our study provides the preliminary empirical evidence indicating their relationships. We found that enhanced inhibitory activity in the frontoparietal network was accompanied by higher frequency connectivity between the frontal and parietal areas. At the behavioral level, we found a marginally significant correlation between the magnitude of IOR and the speed of attentional sampling induced by visible cues. Therefore, we speculate that the top-down inhibition signal originating from the frontal region may be linked to dynamic changes in the connections

between top-down and bottom-up attention systems, supporting both suppression of irrelevant information and accelerated sampling in space.

Our assumption may be supported by the excitatory-inhibitory balance within the neural circuit. The balance between the mean recurrent excitation and inhibition of neural circuits is essential to the properties of neural oscillations⁶⁹. Previous studies have shown that increased inhibitory neurotransmitters result in faster neural oscillations⁷⁰. Furthermore, recurrent neural dynamics related to the conscious representations of stimuli were found to be necessary for long-range inhibition⁷¹. We speculate that this consciousness-dependent inhibitory activity could change the excitatory-inhibitory balance in the attention network, leading to the enhanced alpha oscillations. A neural modeling study has also demonstrated that modifying the excitatory-inhibitory ratio of neural circuits alters the sampling rate of the simulated attention network⁷². However, this hypothesis requires further validation through direct neural evidence.

In conclusion, our findings provide evidence that attention samples space rhythmically, regardless of cue awareness, supporting the idea that this is an inherent property of attention. More importantly, our results indicate that the presence or absence of conscious representation of visual stimuli significantly influences the temporal dynamics of attentional sampling. We propose that further comparisons of neural oscillation patterns at different levels of consciousness using other neuroelectrophysiological techniques are necessary. This approach could offer insights into the relationship between attention and consciousness, aiding in the understanding of the complexities underlying various attentional dysfunctions.

Methods

Subjects

Forty-two subjects took part in the study, with twenty (10 females, mean age 24.5 ± 2.8) participating in Experiment 1 (behavioral task) and twenty-two (10 females, mean age 24.2 ± 3.1) participating in Experiment 2 (EEG task). The sample size was determined based on previous studies investigating attentional rhythms using similar tasks, which typically involved 14 to 16 participants. Increasing the sample size to around 20 ensured $\geq 95\%$ power to detect cue awareness-modulated differences (estimated using G-Power 3.1; $\alpha = 0.05$, effect size $d = 0.85$). The EEG experiment employed the same sample size as the behavioral study to maintain consistency. All subjects were right-handed with normal or corrected-to-normal vision and were naïve to the study. They provided written informed consent and received monetary compensation. The study protocols were approved by the institutional review board of the Institute of Psychology, Chinese Academy of Sciences.

Stimuli and procedure of Experiment 1

Subjects performed the task in a dimly lit room, with their head stabilized by a chin rest positioned 57 cm from the monitor. Stimuli were displayed on a 24-inch CRT monitor (1920 × 1080 pixels at 60 Hz) using Psychtoolbox extensions⁷³ for MATLAB (MathWorks Inc., Natick, MA).

The task followed the general procedure of a Posner-cueing paradigm (Fig. 1a). Subjects were instructed to maintain fixation at the central cross ($0.5^\circ \times 0.5^\circ$) and covertly attend to two peripheral boxes ($5^\circ \times 5^\circ$) presented 5.6° on either side of the fixation cross. After a random duration of 600–1000 ms, a spatial cue ($1.5^\circ \times 1.5^\circ$) was presented 7° away from the fixation cross for 100 ms. This cue randomly appeared on the left or right with equal likelihood to reset the sampling of attention. Subsequently, 100–1000 ms after the cue onset (cue-to-target SOA), a target (a white line tilted either $+45^\circ$ or -45° from the vertical position, $0.8^\circ \times 0.15^\circ$) was presented for 33 ms at the center of either the left or the right boxes. The target was presented on either the same (cued) or the opposite (uncued) location as the cue with a 50% congruency. Upon the appearance of the target, subjects

were required to discriminate the orientation of the target and respond by pressing the predefined key as quickly and accurately as possible. A time-resolved measurement was adopted to densely sample their behavioral performance^{5,16,29,36}. Specifically, the target stimulus appeared at one of 28 temporal intervals from 100 ms to 1000 ms after cue onset in steps of 33 ms, corresponding to a sampling frequency of 30 Hz.

We manipulated the visual awareness of cues using the CFF technique, wherein two oppositely colored stimuli were alternately presented at a temporal frequency surpassing the fusion threshold (~30 Hz). The screen background was filled with a yellow hue (RGB [134, 151, 0]) at a luminance of 34.14 cd/m². The cues consisted of two anti-phased red-green sinusoidal grating discs (horizontally oriented, spatial frequency of 2.7 c/°, mean intensity = 134 for the red channel, and 151 for the green channel). In the visible condition, one of the two discs was randomly selected and consistently presented. In the invisible condition, the two discs alternated and flickered at a frequency of 30 Hz, appearing as a fused yellow disc and rendering them indistinguishable from the background.

The visible and invisible conditions were divided into two sessions with an equal number of trials and presented in a counterbalanced order across participants. Each subject completed 2 (target location: cued vs. uncued) × 28 (SOA: 100:33:1000 ms) × 20 repetitions, totaling 1120 trials in each session. Before the first session, subjects were familiarized with the task through a block of practice and learned to maintain fixation. The experimental conditions of each trial were pseudorandomized. A 1-min break was taken every 32 trials to mitigate fatigue effects. To minimize the influence of top-down expectation about cue validity, subjects were informed that the cues were irrelevant to the tasks before each session.

Stimuli and procedure of Experiment 2

The experimental settings for Experiment 2 remained consistent with those of Experiment 1, except that the subjects completed the task in a darkened room. This environmental adjustment was intended to elicit heightened neural responses to visual stimuli with varying luminance levels.

Experiment 2 employed a Posner cueing task (Fig. 1b) as well. Each trial began with the presentation of a central cross (0.5° × 0.5°) and two white discs (5.5° × 5.5°) positioned 7.5° on either side of the cross, lasting for 1000 ms. Then, the attentional cue consisting of four anti-phased red-green sinusoidal gratings (1.2° × 1.2°, spatial frequency of 3.3 c/°) appeared around one of the discs for 200 ms. Each grating was centered 0.64° away from the edge of the disc. Cue awareness was manipulated as in Experiment 1. In the visible condition, one red-green sinusoidal grating was randomly selected and continuously presented. In the invisible condition, two anti-phased gratings alternated at 30 Hz, rendering the cue imperceptible against the background.

At cue onset, both placeholder discs began flickering and continued for 5 s. Although the cue and discs flickered synchronously—potentially attenuating the overall cueing effect—this setup ensured no bias between conditions¹⁷. To extract the object-specific neural impulse response using the TRF approach, the luminance of each disc was modulated frame-by-frame with independently generated random sequences for each trial. Each sequence was constructed to have equal power across all frequencies by normalizing the amplitude of its Fourier components and then applied the inverse Fourier transform^{17,74}. These luminance sequences, ranging from 0.75 cd/m² to 80.73 cd/m², produced a strong perceptual flicker. With a CRT refresh rate of 60 Hz, we were able to capture stimulus-driven responses in the frequency range of 0–30 Hz.

Subjects were instructed to maintain fixation on the cross and covertly detect the appearance of a target square (3.75° × 3.75°) within one of the two discs. The target square was presented for 500 ms in 25% of all EEG trials at a uniformly distributed random time between

200 ms and 4200 ms throughout the entire trial. At the end of each trial, subjects indicated whether they had detected the target by pressing predefined keys. To maintain a target detection performance of ~80% upon its appearance, the luminance of the target relative to the momentary disc luminance was adjusted across trials using a 3-down-1-up staircase procedure. This design ensured that subjects continuously sustained their attention on the discs, allowing for the examination of dynamic attentional fluctuations.

The EEG experiment was divided into visible and invisible sessions, each consisting of 256 trials (two locations each with 128 repetitions). Before the formal tasks, subjects practiced about 16 trials to familiarize themselves with task execution, maintaining fixation, and controlling eye blinks. Additionally, they took 2–3 min rest breaks after every 16 trials. The eye movements were monitored using electrooculograms.

Awareness check

After each session, the subjects were asked to report whether they perceived any cues before the target's appearance. Furthermore, a two-alternative forced-choice task was conducted as an awareness check for both Experiment 1 and 2. The stimuli and trial procedures closely mirrored those used in Experiments 1 and 2, with the exception that only the invisible cues randomly appeared in the left or right box with equal probability. Subjects were instructed that a stimulus would appear in one of the boxes and that they were to press the left or right key to indicate which box they believed contained the stimulus. If the accuracy of this task is at chance level, it indicates that the cues are processed at an objectively unconscious level²². Individuals who subjectively reported being aware of the cues and performed above chance level in the forced-choice task were excluded.

Behavioral data analysis

Behavioral data were analyzed using MATLAB, employing functions from the EEGLAB toolbox⁷⁵ and CircStat toolbox⁷⁶. In Experiment 1, the accuracy levels approached the ceiling (98.1% ± 0.9%), while in Experiment 2, they were modulated by the staircase procedure (target trial = 79.7% ± 1.5%; non-target trial = 97.2% ± 3.3%), indicating good task performance by the subjects. Task accuracy was not affected by cue awareness (visible vs. invisible), cue congruency (cued vs. uncued), or their interaction (all *p*s > 0.100). Therefore, we employed the reaction time (RT) and the detection threshold of 80% to compute the measures of attention effects for Experiments 1 and 2, respectively.

In Experiment 1, the RTs for correct responses within three standard deviations across all trials were included in our analysis, resulting in the removal of 3.1% and 3.5% of the trials for the visible and the invisible sessions, respectively. We calculated the z-score of RT (RTZ) within each subject separately (i.e., subtracting each subject's mean RT and dividing by their standard deviation) to eliminate potential variance between individuals in overall motor responses. Then, we calculated the cueing effect (CE) by subtracting cued RTZ from uncued RTZ across all SOA conditions for each subject, yielding a time course that depicted the dynamic allocation of attention. From there, we conducted separate analyses on classical attention effects and attentional sampling.

For the classical attention effects, we calculated the 240 ms (8-time bins) moving average of the CE time courses^{16,29} to derive a slowly developed temporal profile. At the same time, we calculated the collapsed CE on the early (100–400 ms) and the late (600–1000 ms) latencies as indices of early facilitation and late inhibition effects, respectively^{32,77}. ANOVA was performed to assess the statistical differences between the visible and invisible conditions. For the attentional sampling, we removed the slowly developing trend by fitting a linear function in the CE time course¹⁰. The detrended CE time course for each subject was tapered using a Hanning window, zero-padded to a length of 64 (matching the NFFT value), and converted into the

frequency domain using FFT^{5,16,29}. The amplitude spectra were computed as twice the absolute value of the FFT output.

As shown in Fig. 2, we performed spectral analysis for each participant individually and then computed the group-averaged spectrum. To evaluate whether the peak spectral power at the group level reached statistical significance, we focused on the 2–12 Hz frequency range, which encompasses the core frequency band where behavioral oscillations have been commonly reported. To determine whether observed peaks reflected genuine periodic oscillations rather than aperiodic components, we adopted the method proposed by Brookshire¹⁰. Specifically, we fitted each participant's aperiodic component of the attentional time series using an autoregressive (AR) model. Based on these models, we generated 1000 surrogate datasets with added noise that preserved the aperiodic structure while eliminating periodic contributions. The group-averaged spectrum of these surrogates served as a null distribution, from which we extracted the maximum power value across frequencies to establish a multiple-comparison corrected threshold at the $p=0.05$ (one-tailed) significance level^{16,29,78}. Spectral peaks exceeding this threshold were thus considered statistically significant rhythmic components.

In addition, we implemented a randomization-based approach by shuffling each participant's time series 1000 times to create another null distribution. This method tested whether the signal contained any consistent temporal structure⁷. By comparing the experimental spectral peaks to both null distributions, we determined whether attentional fluctuations reflected true periodicity or merely stable time-locked components. To further compare the dominant sampling frequencies between the visible and invisible conditions, we identified, for each participant, the frequency with the highest power within the 3–10 Hz range as the individual's peak attentional sampling frequency. These frequencies were then statistically compared across conditions using a two-tailed paired t -test.

To further determine whether the oscillation pattern of the CE time course could reflect the sequential attentional sampling between cued and uncued locations, we analyzed the oscillation component of RTZ_{cued} and RTZ_{uncued} time courses separately and the phase relationship between them. Spectrum analyses were conducted using the same pipeline as for the cueing effect. The only modification involved applying a quadratic detrending procedure to remove nonlinear preparatory trends commonly observed in RT data⁷⁹. We computed the phase lag within the peak frequency range of CE and employed the Rayleigh test to assess the consistency of the phase lag across subjects⁷. To further examine whether participants' phase lags were significantly clustered around 180°—indicating an antiphase relationship—we employed the V-test, a circular statistical method used to assess whether phase angles are non-uniformly distributed around a specified mean direction. For the phase analysis, we selected the time range from 130 ms to 800 ms to circumvent the interference of early and late noise¹⁶. Watson's U2 tests⁸⁰ were conducted to compare the phase distribution difference between visible and invisible conditions⁸¹.

In Experiment 2, we introduced the target square in a small subset of trials to sustain subjects' attention. We used the maximum likelihood method to fit the performance obtained by the staircase procedure, yielding a contrast threshold for subjects to accurately detect the presence of the target at an 80% correct rate⁸². Additionally, we computed the difference between the thresholds under cued and uncued conditions as an indicator of cueing effect.

EEG recording

The EEG was recorded at 500 Hz using a SynAmps2 NeuroScan amplifier System with 64 Ag-AgCl electrodes positioned in accordance with the international 10-20 system. Additionally, Horizontal and vertical electrooculograms were captured by four additional electrodes

placed around the subjects' eyes. Impedances for all electrodes were maintained below 8 k Ω .

EEG preprocessing

The preprocessing was carried out in the MATLAB environment using the EEGLAB toolbox⁷⁵. EEG recordings were band-pass filtered between 2 and 50 Hz, and segmented into epochs lasting for 5.5 s, starting from 0.5 s before cue onset. These epochs were referenced to the averaged value of all channels and visually inspected to exclude trials contaminated with excessive noise. The removal rate did not differ between the visible and invisible sessions (1.8% vs. 2.5%, $\chi^2=0.22$, $p=0.637$). Following trial rejection, independent component analysis was applied to remove artifact components. The cleaned data were subjected to anti-aliasing filtering (i.e., low-pass filtered below 30 Hz), baseline-corrected using the 500–0 ms pre-cue interval, and down-sampled to 60 Hz. To eliminate the influence of onset and offset responses, the EEG and stimulus sequences from the first 500 ms after cue onset and 500 ms before disc offset were not included in the estimation of the TRF¹⁷.

TRF estimation

The TRF was calculated using the multivariate temporal response function (mTRF) toolbox⁸³. Specifically, the luminance values and EEG data from trials where the target did not appear were concatenated across trials and then normalized. The TRF of each condition (2 cue awareness levels \times 2 locations), each channel, and each subject was estimated separately as a function of temporal lag (–100 to 1000 ms) through a regularized linear regression between the stimuli luminance value and EEG amplitude. We maintained a consistent lambda value of 1 for all subjects to control overfitting in the ridge regression. It is noteworthy that the time axis of the TRF indicates a relative temporal relationship between the unit change in the luminance of the stimuli and the EEG after a specific latency, rather than the absolute EEG time course⁸⁴.

Time-frequency analysis

The obtained TRF responses were analyzed using the wavelet toolbox and the FieldTrip toolbox function⁸⁵ within MATLAB. Each TRF temporal profile was transformed using the continuous complex Gaussian wavelet using the CWT function ('cgau4'), with frequencies ranging from 1 to 30 Hz in 1 Hz increments. This method offers better frequency resolution than discrete wavelet transforms, and maintains the same time resolution as the original data in each frequency band. Power was extracted from the resulting complex time series by squaring the absolute value. Theta and alpha powers were calculated by averaging the power within the 3–7 Hz and 8–12 Hz ranges, respectively, and then normalized by subtracting the average power during the baseline period (–100 to 0 ms) from the power at each time point.

We first averaged the TRF oscillatory activity across all experimental conditions (i.e., cue awareness and cue congruency), electrodes, and time points. We then identified the time of interest (TOI: 117–383 ms) during which the response exceeded twice the mean amplitude, allowing us to focus our analysis on a data-driven time window with the strongest overall signal. The difference in oscillation power between cued and uncued conditions at different frequency bands within the TOI was compared using cluster-based permutation tests ($n=1000$, $p<0.05$ for all clusters, two-tailed). To address the central question of how cue awareness modulates attentional neural dynamics, we compared the alpha power cueing effects (cued minus uncued power) between the visible and invisible conditions, both within the predefined TOI and across the entire 0–1000 ms time window. For all cluster-based permutation tests, we employed the maximum-cluster statistic ('montecarlo') to correct for multiple comparisons.

We selected the channel clusters showing robust differences between the visible and invisible conditions as COI and calculated the average cueing effects within these clusters. To further examine the time course of cueing effects for each condition across the different clusters, point-by-point two-tailed *t*-tests against zero were performed for each condition and cluster separately. Multiple comparisons were corrected using the false discovery rate (FDR). Time windows demonstrating significant alpha modulation differences between conditions were selected (167–267 ms) for Pearson correlation analysis (two-tailed) with behavioral performance.

Connectivity analysis

To further investigate the connectivity between the regions associated with alpha power modulation, we conducted phase coherence analysis and Granger causality analysis. We individually extracted channels from the COI clusters, conducted pairwise analysis, and averaged the results of all pairs to obtain the overall connectivity between the clusters.

Previous research has shown that the connectivity between brain regions can result in a clustering of phase values of neural oscillation relative to an experimental event over repeated trials^{86,87}, which can be quantified using the PLV. We extracted the phase angle at each time point from the complex value obtained by wavelet convolution and calculated the PLV value as follows:

$$PLV_f = \left| N^{-1} \sum_{n=1}^N e^{i(\phi_x - \phi_y)} \right|, \quad (1)$$

with n refers to the number of subjects, and ϕ_x and ϕ_y refer to phase angles from channel x and y at frequency f . In traditional PLV calculations, n typically refers to the number of trials. However, since the TRF method yields only one TRF per subject, it is not feasible to compute PLV across multiple trials. Therefore, we adapted the formula to assess phase consistency across subjects rather than trials, allowing us to evaluate the inter-subject phase alignment of the TRF. A higher PLV indicates stronger network connectivity. We subtracted the PLV strength from the baseline period (–100 to 0 ms) to emphasize the cue-related effects.

To test for statistical significance, we compared the PLV between cued and uncued conditions for visible and invisible cues separately using a non-parametric randomization procedure. We shuffled the TRFs between cue conditions 1000 times and recalculated the difference in PLV, generating a reference distribution. The maximum pixel-based statistics⁸⁸ were applied to correct for multiple comparisons across time and frequency ($p = 0.025$, two-tailed).

After observing increased connectivity in specific conditions and time periods, we performed Granger causality analysis⁸⁹ to determine the strength and direction of influence between the two regions. We computed the Granger prediction in the frequency domain using the TRF time profiles for cued conditions (invisible: 400–900 ms; visible: 100–600 ms). To assess statistical significance, we randomized the selected TRF temporal profiles 1000 times and applied the maximum threshold value to correct for multiple comparisons ($p = 0.05$, two-tailed).

Reporting summary

Further information on research design is available in the Nature Portfolio Reporting Summary linked to this article.

Data availability

The data supporting the findings of this study are fully available within the paper and its Supplementary Information. The source data are openly accessible and provided with this paper. The raw individual-level data are protected due to privacy concerns and intellectual property considerations. Access to these raw data can be granted upon

request by contacting the corresponding author and providing a clear statement of intended data use. The data generated in this study have been deposited in the Science Data Bank database under accession address <https://www.scidb.cn/s/eAJFZf>. Source data are provided with this paper.

Code availability

Custom code can be found on the Science Data Bank: <https://www.scidb.cn/s/eAJFZf>.

References

1. Posner, M. I. Orienting of attention. *Q. J. Exp. Psychol.* **32**, 3–25 (1980).
2. Fiebelkorn, I. C. & Kastner, S. A rhythmic theory of attention. *Trends Cogn. Sci.* **23**, 87–101 (2019).
3. Fries, P. Rhythmic attentional scanning. *Neuron* **111**, 954–970 (2023).
4. Dugué, L., McLelland, D., Lajoux, M. & VanRullen, R. Attention searches nonuniformly in space and in time. *Proc. Natl Acad. Sci.* **112**, 15214–15219 (2015).
5. Fiebelkorn, I. C., Saalman, Y. B. & Kastner, S. Rhythmic sampling within and between objects despite sustained attention at a cued location. *Curr. Biol.* **23**, 2553–2558 (2013).
6. Gaillard, C. et al. Prefrontal attentional saccades explore space rhythmically. *Nat. Commun.* **11**, 925 (2020).
7. Landau, A. N. & Fries, P. Attention samples stimuli rhythmically. *Curr. Biol.* **22**, 1000–1004 (2012).
8. VanRullen, R. Attention cycles. *Neuron* **99**, 632–634 (2018).
9. Fiebelkorn, I. C. & Kastner, S. Functional specialization in the attention network. *Annu. Rev. Psychol.* **71**, 221–249 (2020).
10. Brookshire, G. Putative rhythms in attentional switching can be explained by aperiodic temporal structure. *Nat. Hum. Behav.* **6**, 1280–1291 (2022).
11. Jensen, O., Bonnefond, M. & VanRullen, R. An oscillatory mechanism for prioritizing salient unattended stimuli. *Trends Cogn. Sci.* **16**, 200–206 (2012).
12. Busch, N. A., Dubois, J. & VanRullen, R. The phase of ongoing EEG oscillations predicts visual perception. *J. Neurosci.* **29**, 7869–7876 (2009).
13. Dugué, L., Marque, P. & VanRullen, R. The phase of ongoing oscillations mediates the causal relation between brain excitation and visual perception. *J. Neurosci.* **31**, 11889–11893 (2011).
14. Fiebelkorn, I. C., Pinsk, M. A. & Kastner, S. A dynamic interplay within the frontoparietal network underlies rhythmic spatial attention. *Neuron* **99**, 842–853 (2018).
15. Helfrich, R. F. et al. Neural mechanisms of sustained attention are rhythmic. *Neuron* **99**, 854–865.e5 (2018).
16. Song, K., Meng, M., Chen, L., Zhou, K. & Luo, H. Behavioral oscillations in attention: rhythmic α pulses mediated through θ band. *J. Neurosci.* **34**, 4837–4844 (2014).
17. Jia, J., Liu, L., Fang, F. & Luo, H. Sequential sampling of visual objects during sustained attention. *PLoS Biol.* **15**, e2001903 (2017).
18. VanRullen, R. Perceptual cycles. *Trends Cogn. Sci.* **20**, 723–735 (2016).
19. Noah, S. & Mangun, G. R. Recent evidence that attention is necessary, but not sufficient, for conscious perception. *Ann. N. Y. Acad. Sci.* **1464**, 52–63 (2020).
20. Prasad, S. & Mishra, R. K. The nature of unconscious attention to subliminal cues. *Vision* **3**, 38 (2019).
21. Mashour, G. A., Roelfsema, P., Changeux, J.-P. & Dehaene, S. Conscious processing and the global neuronal workspace hypothesis. *Neuron* **105**, 776–798 (2020).
22. Lamme, V. A. F. Visual functions generating conscious seeing. *Front. Psychol.* **11**, 83 (2020).
23. Chen, Y. et al. Rapid unconscious acquisition of conditioned fear with low-spatial-frequency but emotionally neutral stimuli. *Research* <https://doi.org/10.34133/research.0181> (2023).

24. Fogelson, S. V., Kohler, P. J., Miller, K. J., Granger, R. & Tse, P. U. Unconscious neural processing differs with method used to render stimuli invisible. *Front. Psychol.* <https://doi.org/10.3389/fpsyg.2014.00601> (2014).
25. Jiang, Y., Zhou, K. & He, S. Human visual cortex responds to invisible chromatic flicker. *Nat. Neurosci.* **10**, 657–662 (2007).
26. Liu, D., Liu, W., Yuan, X. & Jiang, Y. Conscious and unconscious processing of ensemble statistics oppositely modulate perceptual decision-making. *Am. Psychol.* **78**, 346–357 (2023).
27. Yang, F. et al. Unconscious and conscious gaze-triggered attentional orienting: distinguishing innate and acquired components of social attention in children and adults with autistic traits and autism spectrum disorders. *Research.* <https://doi.org/10.34133/research.0417> (2024).
28. Lalor, E. C., Pearlmutter, B. A., Reilly, R. B., McDarby, G. & Foxe, J. J. The VESPA: a method for the rapid estimation of a visual evoked potential. *NeuroImage* **32**, 1549–1561 (2006).
29. Huang, Y., Chen, L. & Luo, H. Behavioral oscillation in priming: competing perceptual predictions conveyed in alternating theta-band rhythms. *J. Neurosci.* **35**, 2830–2837 (2015).
30. Lu, S., Cai, Y., Shen, M., Zhou, Y. & Han, S. Alerting and orienting of attention without visual awareness. *Conscious. Cogn.* **21**, 928–938 (2012).
31. Zhang, F., Lin, Z., Zhang, Y. & Zhang, M. Behavioral evidence for attention selection as entrained synchronization without awareness. *J. Exp. Psychol. Gen.* **150**, 1710–1721 (2021).
32. Klein, R. M. Inhibition of return. *Trends Cogn. Sci.* **4**, 138–147 (2000).
33. Dugué, L., Roberts, M. & Carrasco, M. Attention reorients periodically. *Curr. Biol.* **26**, 1595–1601 (2016).
34. Michel, R., Dugué, L. & Busch, N. A. Distinct contributions of alpha and theta rhythms to perceptual and attentional sampling. *Eur. J. Neurosci.* **55**, 3025–3039 (2021).
35. Senoussi, M., Moreland, J. C., Busch, N. A. & Dugué, L. Attention explores space periodically at the theta frequency. *J. Vis.* **19**, 22 (2019).
36. Fries, P. Rhythms for cognition: communication through coherence. *Neuron* **88**, 220–235 (2015).
37. Fiebelkorn, I. C., Pinsk, M. A. & Kastner, S. The mediodorsal pulvinar coordinates the macaque fronto-parietal network during rhythmic spatial attention. *Nat. Commun.* **10**, 215 (2019).
38. Chen, A., Wang, A., Wang, T., Tang, X. & Zhang, M. Behavioral oscillations in visual attention modulated by task difficulty. *Front. Psychol.* **8**, 1630 (2017).
39. Jiang, Y., He, S. & Zhang, J. The adaptive flexibility of rhythmic attentional sampling in attending to multiple targets. *J. Exp. Psychol. Gen.* **153**, 26–37 (2023).
40. Merholz, G., Grabot, L., VanRullen, R. & Dugué, L. Periodic attention operates faster during more complex visual search. *Sci. Rep.* **12**, 6688 (2022).
41. Petersen, S. E. & Posner, M. I. The attention system of the human brain: 20 years after. *Annu. Rev. Neurosci.* **35**, 73–89 (2012).
42. Jensen, O. & Mazaheri, A. Shaping functional architecture by oscillatory alpha activity: gating by inhibition. *Front. Hum. Neurosci.* <https://doi.org/10.3389/fnhum.2010.00186> (2010).
43. Gaspelin, N. & Luck, S. J. The role of inhibition in avoiding distraction by salient stimuli. *Trends Cogn. Sci.* **22**, 79–92 (2018).
44. Moorselaar, D. & Slagter, H. A. Inhibition in selective attention. *Ann. N. Y. Acad. Sci.* **1464**, 204–221 (2020).
45. Bouret, S. & Sara, S. J. Network reset: a simplified overarching theory of locus coeruleus noradrenergic function. *Trends Neurosci.* **28**, 574–582 (2005).
46. Jefferies, L. N. & Di Lollo, V. Sudden events change old visual objects into new ones: a possible role for phasic activation of Locus Coeruleus. *Psychol. Sci.* **30**, 55–64 (2019).
47. Feng, W., Störmer, V. S., Martinez, A., McDonald, J. J. & Hillyard, S. A. Involuntary orienting of attention to a sound desynchronizes the occipital alpha rhythm and improves visual perception. *NeuroImage* **150**, 318–328 (2017).
48. Foxe, J. J., Simpson, G. V. & Ahlfors, S. P. Parieto-occipital -10Hz activity reflects anticipatory state of visual attention mechanisms. *NeuroReport* **9**, 3929–3933 (1998).
49. Foxe, J. J. & Snyder, A. C. The role of alpha-band brain oscillations as a sensory suppression mechanism during selective attention. *Front. Psychol.* **2**, 154 (2011).
50. Sauseng, P. et al. A shift of visual spatial attention is selectively associated with human EEG alpha activity. *Eur. J. Neurosci.* **22**, 2917–2926 (2005).
51. Snyder, A. C. & Foxe, J. J. Anticipatory attentional suppression of visual features indexed by oscillatory alpha-band power increases: a high-density electrical mapping study. *J. Neurosci.* **30**, 4024–4032 (2010).
52. Worden, M. S., Foxe, J. J., Wang, N. & Simpson, G. V. Anticipatory biasing of visuospatial attention indexed by retinotopically specific α -band electroencephalography increases over occipital cortex. *J. Neurosci.* **20**, RC63–RC63 (2000).
53. Jia, J., Fang, F. & Luo, H. Selective spatial attention involves two alpha-band components associated with distinct spatiotemporal and functional characteristics. *NeuroImage* **199**, 228–236 (2019).
54. Corbetta, M. & Shulman, G. L. Spatial neglect and attention networks. *Annu. Rev. Neurosci.* **34**, 569–599 (2011).
55. Shulman, G. L. et al. Right hemisphere dominance during spatial selective attention and target detection occurs outside the dorsal frontoparietal network. *J. Neurosci.* **30**, 3640–3651 (2010).
56. de Schotten, M. et al. A lateralized brain network for visuospatial attention. *Nat. Neurosci.* **14**, 1245–1246 (2011).
57. Zou, J., He, S. & Zhang, P. Binocular rivalry from invisible patterns. *Proc. Natl Acad. Sci.* **113**, 8408–8413 (2016).
58. Uddin, L. Q. Saliency processing and insular cortical function and dysfunction. *Nat. Rev. Neurosci.* **16**, 55–61 (2015).
59. Wang, L. et al. An awareness-dependent mapping of saliency in the human visual system. *NeuroImage* **247**, 118864 (2022).
60. Zhang, X., Zhaoping, L., Zhou, T. & Fang, F. Neural activities in V1 create a bottom-up saliency map. *Neuron* **73**, 183–192 (2012).
61. Zhaoping, L. From the optic tectum to the primary visual cortex: migration through evolution of the saliency map for exogenous attentional guidance. *Curr. Opin. Neurobiol.* **40**, 94–102 (2016).
62. Ekstrom, L. B., Roelfsema, P. R., Arsenault, J. T., Bonmassar, G. & Vanduffel, W. Bottom-up dependent gating of frontal signals in early visual cortex. *Science* **321**, 414–417 (2008).
63. Gregoriou, G. G., Gotts, S. J., Zhou, H. & Desimone, R. High-frequency, long-range coupling between prefrontal and visual cortex during attention. *Science* **324**, 1207–1210 (2009).
64. Martinez-Trujillo, J. Visual attention in the prefrontal cortex. *Annu. Rev. Vis. Sci.* **8**, 407–425 (2022).
65. Helfrich, R. F. & Knight, R. T. Oscillatory dynamics of prefrontal cognitive control. *Trends Cogn. Sci.* **20**, 916–930 (2016).
66. Lobier, M., Palva, J. M. & Palva, S. High-alpha band synchronization across frontal, parietal and visual cortex mediates behavioral and neuronal effects of visuospatial attention. *NeuroImage* **165**, 222–237 (2018).
67. Dehaene, S., Sergent, C. & Changeux, J.-P. A neuronal network model linking subjective reports and objective physiological data during conscious perception. *Proc. Natl Acad. Sci.* **100**, 8520–8525 (2003).
68. Bourgeois, A., Chica, A. B., Migliaccio, R., de Schotten, M. T. & Bartolomeo, P. Cortical control of inhibition of return: evidence from patients with inferior parietal damage and visual neglect. *Neuropsychologia* **50**, 800–809 (2012).

69. Brunel, N. & Wang, X.-J. What determines the frequency of fast network oscillations with irregular neural discharges? I. Synaptic dynamics and excitation-inhibition balance. *J. Neurophysiol.* **90**, 415–430 (2003).
70. Whittington, M. A., Traub, R. D., Kopell, N., Ermentrout, B. & Buhl, E. H. Inhibition-based rhythms: experimental and mathematical observations on network dynamics. *Int. J. Psychophysiol.* **38**, 315–336 (2000).
71. Northoff, G. & Lamme, V. Neural signs and mechanisms of consciousness: Is there a potential convergence of theories of consciousness in sight?. *Neurosci. Biobehav. Rev.* **118**, 568–587 (2020).
72. Chen, G. & Gong, P. A spatiotemporal mechanism of visual attention: superdiffusive motion and theta oscillations of neural population activity patterns. *Sci. Adv.* **8**, eabl4995 (2022).
73. Brainard, D. H. The psychophysics toolbox. *Spat. Vis.* **10**, 433–436 (1997).
74. Lozano-Soldevilla, D. & VanRullen, R. The hidden spatial dimension of alpha: 10-Hz perceptual echoes propagate as periodic traveling waves in the human brain. *Cell Rep.* **26**, 374–380.e4 (2019).
75. Delorme, A. & Makeig, S. EEGLAB: an open source toolbox for analysis of single-trial EEG dynamics including independent component analysis. *J. Neurosci. Methods* **134**, 9–21 (2004).
76. Berens, P. CircStat: a MATLAB toolbox for circular statistics. *J. Stat. Softw.* **31**, 1–21 (2009).
77. Lupiáñez, J., Milán, E. G., Tornay, F. J., Madrid, E. & Tudela, P. Does IOR occur in discrimination tasks? Yes, it does, but later. *Percept. Psychophys.* **59**, 1241–1254 (1997).
78. Nichols, T. E. & Holmes, A. P. Nonparametric permutation tests for functional neuroimaging: a primer with examples. *Hum. Brain Mapp.* **15**, 1–25 (2002).
79. Wang, M., Huang, Y., Luo, H. & Zhang, H. Sustained visual priming effects can emerge from attentional oscillation and temporal expectation. *J. Neurosci.* **40**, 3657–3674 (2020).
80. Watson, G. S. Goodness-of-fit tests on a circle. *Biometrika* **48**, 109–114 (1961).
81. Landler, L., Ruxton, G. D. & Malkemper, E. P. Advice on comparing two independent samples of circular data in biology. *Sci. Rep.* **11**, 20337 (2021).
82. Wichmann, F. A. & Hill, N. J. The psychometric function: I. Fitting, sampling, and goodness of fit. *Percept. Psychophys.* **63**, 1293–1313 (2001).
83. Crosse, M. J., Di Liberto, G. M., Bednar, A. & Lalor, E. C. The Multi-variate Temporal Response Function (mTRF) Toolbox: A MATLAB toolbox for relating neural signals to continuous stimuli. *Front. Hum. Neurosci.* <https://doi.org/10.3389/fnhum.2016.00604> (2016).
84. Lalor, E. C. Modeling the human visual system using the white-noise approach. In *Proc. 2009 4th International IEEE/EMBS Conference on Neural Engineering* 589–592 (IEEE, Antalya, Turkey, 2009) <https://doi.org/10.1109/NER.2009.5109365>.
85. Oostenveld, R., Fries, P., Maris, E. & Schoffelen, J.-M. FieldTrip: open source software for advanced analysis of MEG, EEG, and invasive electrophysiological data. *Comput. Intell. Neurosci.* **2011**, 1–9 (2011).
86. Lachaux, J., Rodriguez, E., Martinerie, J. & Varela, F. J. Measuring phase synchrony in brain signals. *Hum. Brain Mapp.* **8**, 194–208 (1999).
87. Makeig, S. et al. Dynamic brain sources of visual evoked responses. *Science* **295**, 690–694 (2002).
88. Cohen, M. X. *Analyzing Neural Time Series Data: Theory and Practice* (MIT Press, 2014).
89. Granger, C. W. Investigating causal relations by econometric models and cross-spectral methods. *Econom. J. Econom. Soc.* **37**, 424–438 (1969).

Acknowledgements

This study was supported by grants from the Ministry of Science and Technology of China (2021ZD0203800 to Y.J. and 2021ZD0204200 to S.H.), the National Natural Science Foundation of China (32430043 to Y.J.), the Key Research and Development Program of Guangdong (2023B0303010004 to Y.J.), the Interdisciplinary Innovation Team of the Chinese Academy of Sciences (JCTD-2021-06 to Y.J.), Fundamental Research Funds for the Central Universities (to Y.J.), and the National Social Science Fund of China (2023-SKJJ-O-B-001 to F.Y.).

Author contributions

All authors contributed to the study's design and conceptualization. F.Y., P.J.Y., and Y.J. conceived the original idea. F.Y., P.J.Y., and L.S. conducted the experiments and collected the data. F.Y., P.J.Y., L.S., and K.Z. analyzed and interpreted the data, under the guidance of S.H. and Y.J. All authors participated in manuscript preparation and approved the final version for submission.

Competing interests

The authors declare no competing interests.

Additional information

Supplementary information The online version contains supplementary material available at <https://doi.org/10.1038/s41467-025-64987-7>.

Correspondence and requests for materials should be addressed to Yi Jiang.

Peer review information *Nature Communications* thanks Geoffrey Brookshire, Jianrong Jia and the other, anonymous, reviewer(s) for their contribution to the peer review of this work. A peer review file is available.

Reprints and permissions information is available at <http://www.nature.com/reprints>

Publisher's note Springer Nature remains neutral with regard to jurisdictional claims in published maps and institutional affiliations.

Open Access This article is licensed under a Creative Commons Attribution-NonCommercial-NoDerivatives 4.0 International License, which permits any non-commercial use, sharing, distribution and reproduction in any medium or format, as long as you give appropriate credit to the original author(s) and the source, provide a link to the Creative Commons licence, and indicate if you modified the licensed material. You do not have permission under this licence to share adapted material derived from this article or parts of it. The images or other third party material in this article are included in the article's Creative Commons licence, unless indicated otherwise in a credit line to the material. If material is not included in the article's Creative Commons licence and your intended use is not permitted by statutory regulation or exceeds the permitted use, you will need to obtain permission directly from the copyright holder. To view a copy of this licence, visit <http://creativecommons.org/licenses/by-nc-nd/4.0/>.

© The Author(s) 2025